

An Initial Assessment of Navier-Stokes Codes Applied to Supersonic Retro-Propulsion

Kerry A. Trumble*

NASA Ames Research Center, Moffett Field, California, 94035

Daniel G. Schauerhamer†

Jacobs Technology, Houston, Texas, 77058

William Kleb‡, Jan-Renee Carlson§, Pieter G. Buning** and Karl Edquist††

NASA Langley Research Center, Hampton, Virginia, 23681

Michael D. Barnhardt‡‡

ELORET Corp, Sunnyvale, California, 94086

This paper describes an initial evaluation of Navier-Stokes computational fluid dynamics codes applied to the problem of Supersonic Retro-Propulsion flowfield prediction. A few cases with existing wind tunnel data were selected to evaluate Navier-Stokes codes and build experience running flowfield simulations. Three codes (DPLR, FUN3D, and OVERFLOW) have been exercised for both single and multi-nozzle configurations for a range of Mach numbers and thrust coefficients, all at zero degrees angle-of-attack. Comparisons of surface pressure and flow structure have been used to evaluate the codes and identify modeling strengths and weaknesses. In addition, lessons learned about grid generation, grid adaptation, and solution advancement are reported for each code.

Nomenclature

A_{ref}	=	reference area (m ²)
C_p	=	pressure coefficient
C_T	=	thrust coefficient
d	=	diameter (m)
p	=	pressure (Pa)
q	=	dynamic pressure (Pa)
T	=	thrust (N)
V	=	velocity (m/s)
ρ	=	density (kg/m ³)

* Research Scientist, Aerothermodynamics Branch, MS 230-2, Kerry.A.Trumble@nasa.gov, Senior Member.

† CFD Analyst, Applied Aerosciences and CFD Branch, MS EG-3, Daniel.G.Schauerhamer@nasa.gov, Member.

‡ Aerospace Engineer, Aerothermodynamics Branch, MS 408A, Bil.Kleb@nasa.gov, Senior Member.

§ Aerospace Engineer, Computational Aerosciences Branch, MS 128, Jan-Renee.Carlson@nasa.gov, Senior Member.

** Aerospace Engineer, Computational Aerosciences Branch, MS 128, Pieter.G.Buning@nasa.gov, Associate Fellow.

†† Aerospace Engineer, Atmospheric Flight and Entry Systems Branch, MS 489, Karl.T.Edquist@nasa.gov, Senior Member.

‡‡ Research Scientist, Aerothermodynamics Branch, MS 230-3, Michael.D.Barnhardt@nasa.gov, Senior Member.

Subscripts

∞ freestream condition

ref reference condition

I. Introduction

Supersonic Retro-Propulsion (SRP) has been proposed as a means to decelerate Exploration-scale missions (10s of metric tons) to the surface of Mars.¹ Aerodynamics is important for predicting vehicle controllability, and aeroheating determines thermal protection requirements. The advancement of SRP as a technology will be strongly influenced by the use of Navier-Stokes computational fluid dynamics (CFD) to predict aerodynamics and aeroheating during the SRP phase of atmospheric entry.

Historic SRP wind tunnel tests are available to support preliminary CFD assessment and development.² Jarvinen and Adams performed a leading experiment that evaluated both single nozzle and three-nozzle configurations.³ The experiment by Daso et al. is the most recent and is a single nozzle configuration.⁴ The experiment by McGhee looked at plume gas effects on a single nozzle configuration.⁵ A subset of these experiments was chosen to begin evaluation of existing Navier-Stokes codes, build experience running SRP flowfield simulations, and identify shortcomings to be addressed by future development tasks.⁶

Jarvinen and Adams described the characteristics of a single SRP jet flow flowfield in Figure 1. The complex interaction between the jet plume and external flowfield is expected to stress the capabilities of existing CFD codes and will drive further development in numerous areas, including grid generation/adaption and turbulence modeling. Three NASA CFD codes DPLR⁷, OVERFLOW⁸ and FUN3D^{9,10} are being tested for both single and multiple-nozzle configurations for a range of Mach numbers and thrust coefficients. Quantitative (surface pressure, forces and moments) and qualitative (flowfield structure) comparisons will be used to evaluate the codes and identify modeling capabilities. The present paper summarizes an initial assessment of the three codes for SRP, lessons learned, and recommendations for further development.

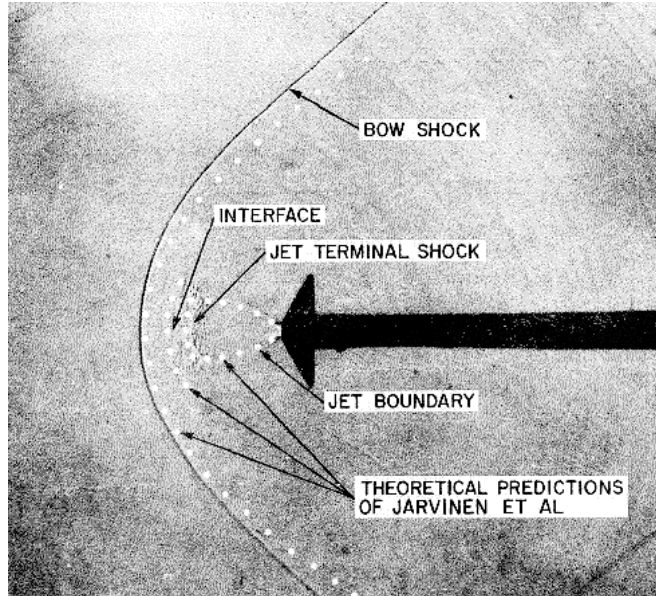


Figure 1: SRP jet plume characteristics described by Jarvinen and Adams for a 60° aeroshell, freestream Mach $M_\infty=2.0$ and thrust coefficient $C_T=1.0$.³

II. Computational Method

CFD is an inexpensive means of determining important design factors such as aerodynamics, aerothermodynamics. These insights are in-turn used to design vehicle systems such as guidance, navigation and control (GN&C) and thermal protection systems on full-scale vehicles. It is important then that the CFD tool's capabilities are well understood. Three different CFD codes utilizing finite-volume or finite-difference methods are employed to assess their respective capabilities for simulating SRP flows: cell-centered structured grid, node-centered overset structured grid, and node-centered unstructured grid. All codes assume perfect gas in the presented results. A brief summary of each code is given below.

A. DPLR

The Data Parallel Line Relaxation (DPLR) CFD code⁷ is a parallel, structured multi-block, finite-volume code that solves the Navier-Stokes equations for continuum flow, including finite-rate chemistry and thermal non-equilibrium. In the present study the equations are solved implicitly in time with first-order accuracy, although DPLR can be run second-order time implicit with sub-iterations. Euler fluxes are computed using modified Steger-Warming flux vector splitting¹¹ with third-order spatial accuracy via MUSCL extrapolation with a minmod limiter.¹² The viscous fluxes are computed with second-order spatial accuracy using a central difference approach. For the present analysis, the Shear-Stress Transport (SST) turbulence model was employed and all simulations were modeled as a perfect gas. The SST model within DPLR is vorticity based. Although DPLR includes OVERSET grid capabilities, the presented results are with point-matched grid systems.

B. FUN3D

The Fully Unstructured Navier-Stokes Three-Dimensional suite of codes (FUN3D) contains a node-based finite-volume flow solver.^{9,10} The FUN3D website, <http://fun3d.larc.nasa.gov>, contains the user manual and an extensive list of references. FUN3D can solve unsteady, incompressible and compressible, Euler and Navier-Stokes flow with thermochemical non-equilibrium. The present study employs Edwards' LDFSS flux function¹³ with a Van Albada limiter¹⁴ to solve the compressible RANS equations coupled to Menter's SST turbulence model.¹⁵ The SST model here is strain based. All node-based conservative variables are computed by driving a second-order accurate spatial residual to steady-state with a point-implicit iterative method. For steady flows, local time stepping is employed and for unsteady flows, up to fourth-order time accuracy is available via sub-iterations. FUN3D can utilize general mixed-element grids and overset grid systems, but only tetrahedral grids are used in this study. Automatic domain decomposition is employed to fully exploit distributed-memory and through using the parallel grid adaptation mechanics by Park and Darmofal, Mach Hessian gradient-based adaptation was used to sharpen flow features.^{16,17}

C. OVERFLOW

OVERFLOW 2⁸ is an implicit Reynolds Averaged Navier-Stokes (RANS) flow solver that utilizes structured overset grids.^{18,19} Several Euler flux schemes are available, including central differencing and a number of upwind schemes.^{20,21} Implicit time advance schemes include block tridiagonal ADI, scalar pentadiagonal ADI²², and SSOR. Newton sub-iteration or dual time stepping can be used for second-order, time-accurate simulations.^{23,24} Turbulence models include Baldwin-Barth²⁵, Spalart-Allmaras²⁶, and SST²⁷. Other OVERFLOW capabilities include automatic domain decomposition and partitioning for parallel processing^{28,29}, automatic off-body grid generation with adaptation^{30,31}, grid sequencing and multigrid, low-mach preconditioning, a full six-degree-of-freedom solver with collision detection^{32,33}, and the ability to solve applications with multiple species. For the current work, HLLC++ with the Van Albada limiter was used for spatial terms, and the SSOR algorithm with simple time stepping for temporal terms. All viscous terms were included, and the strain based SST turbulence model was employed. The overall scheme is second-order accurate in space and first-order in time. The calculation of inviscid fluxes for both the flow solver and turbulence model use third-order accurate MUSCL extrapolation.

III. Historical Wind Tunnel Test Cases

As the interest for landing large vehicles on the surface of Mars with SRP increases, so does the interest in the ability to predict these flows with computational methods because it has the potential to be more economical than flight or wind tunnel testing. Historical wind tunnel tests (Table 1) are being revisited to assess CFD for SRP flows. By benchmarking the CFD and understanding historical wind tunnel experiments, new wind tunnel tests can be designed and aerodynamic effects on the aeroshell can more easily be understood; effects such as

aeroshell angle, number of nozzles, engine thrust, size of nozzles, startup dynamics, nozzle throttling, and gas composition on the aerodynamic loads, stability (static and dynamic), and drag. The CFD will help design focused experiments.

Table 1: Summary of CFD test cases from historical wind tunnel data

Report	Model	Number of Jets	Mach Numbers	Thrust Coefficient, C_T	Data Available
Jarvinen & Adams³	60° sphere-cone 4" diameter	1 and 3	Freestream - 2 Nozzle exit - 4	0, 1, 4, 7	Schlieren, pressure coefficient
Daso⁴	Apollo 4" diameter	1	Freestream - 3.48 Nozzle exit - 1	0.4	Schlieren

A. Jarvinen and Adams

Jarvinen and Adams studied a large array of test conditions on four-inch diameter models in the NASA Ames 6' x 6' supersonic wind tunnel. Both single-nozzle and three-nozzle configurations were tested along with freestream Mach numbers from 0.4 to 2.0, various angles of attack, and thrust coefficients up to 30. This variety allows the CFD cases to gradually increase in geometric and physical complexity. Two different types of interaction were observed to occur between a single jet and freestream: long and short jet penetrations. Short jet penetration is largely steady and has a terminal shock behind the bow shock. Long jet penetration extends upstream through the bow shock into the freestream flow and is highly unsteady. The long jet penetration is seen at low thrust coefficients when the jet exit pressure is on the order of or less than the ambient static pressure otherwise, the short jet interaction dominates.

The Jarvinen and Adams report had several inconsistencies or omissions that made detailed CFD assessment troublesome. For example, the freestream temperature and jet plenum conditions were not reported; and the freestream tunnel pressure reported is below the operating envelope for the tunnel. As a result, the freestream temperature and plenum conditions for the CFD cases were chosen from theoretically derived conditions and most likely not the values the wind tunnel test actually experienced. Not all geometric dimensions, such as those necessary to fully characterize the nozzle throats, were explicitly stated. Finally, experimental and measurement uncertainties in the test data were not provided.

The Jarvinen and Adams test cases selected for this study were of a 60° sphere-cone model with both single-nozzle (Figure 2) and three-nozzle configurations (Figure 3). Both cases considered used air as the nozzle exhaust gas and were at zero angle-of-attack with Mach 2 freestream. The single-nozzle configuration was analyzed at thrust coefficients of 0 and 7. The three-nozzle configuration was analyzed at thrust coefficients of 0, 1, 4 and 7.

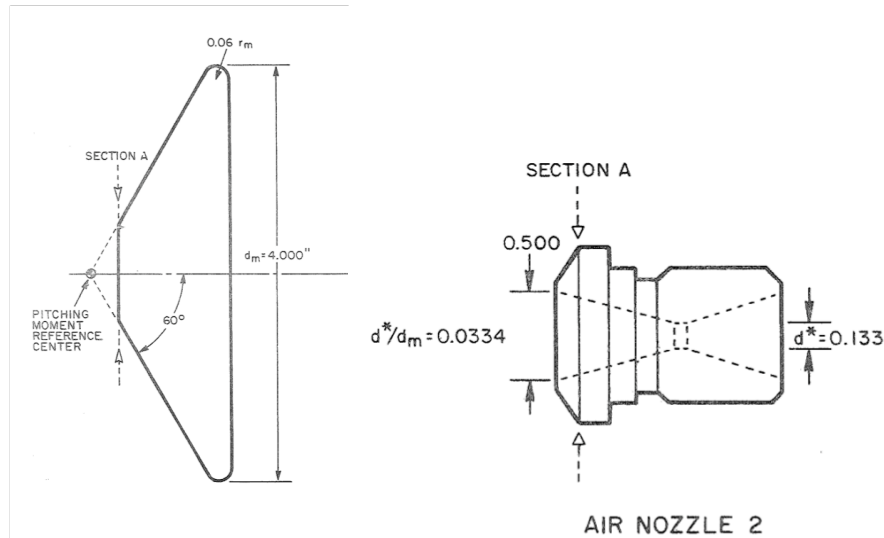


Figure 2: Jarvinen and Adams model and nozzle dimensions.³

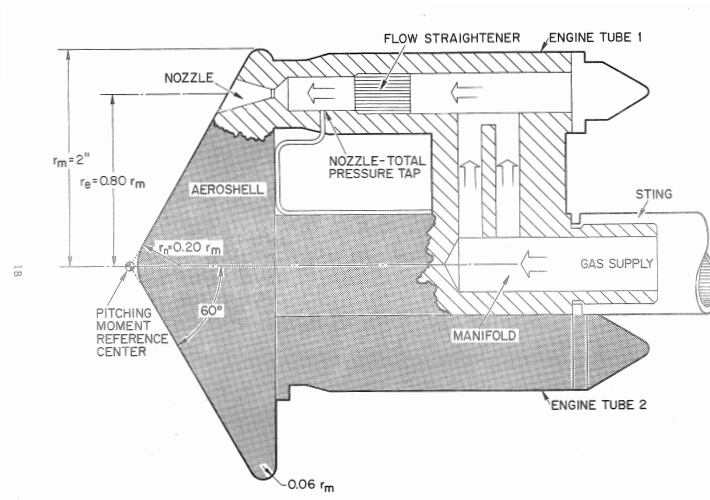


Figure 3: 60° three-nozzle configuration aeroshell model.³

Initial cases with a zero thrust coefficient were first established as a reference for the single-nozzle and three-nozzle geometries. The jet-off cases were run laminar with Reynolds number 1.6×10^5 and experienced steady flow over the forebody. For the jet-on cases, all three codes included turbulence modeling since the Reynolds number of the plume is 1.8×10^6 . Turbulence is generally assumed and modeled above Reynolds number 1×10^6 .

Single-nozzle Configuration

For the single-nozzle configuration the pressure coefficients obtained by the CFD codes agree to within 2% to 16% of the data from Jarvinen and Adams for both $C_T=0$ and 7 (Figure 4). As expected, for the jet off case ($C_T=0$), the CFD solutions agree well with the data and each other. At the shoulder region the codes underpredict the test data by 37%. For the jet on case ($C_T=7$), the DPLR solution agrees with the test data near the shoulder, while FUN3D and OVERFLOW are slightly higher. None of

the codes correctly predict the first data point away from the nozzle, with 180% difference. This could be due to the large amount of separation immediately near the nozzle, which the codes cannot accurately predict, and is likely dominated by uncertainties in the nozzle geometry and test conditions.

The plume structure as predicted by each code is shown using Mach contour plots in Figure 5. The FUN3D simulation is steady while the DPLR and OVERFLOW simulations are unsteady in the plume. In the unsteady simulations the plume pulsed between a barrel shock shape and a plume shape with the terminal shock corners truncated. In the DPLR solution, vortical shedding was seen in the Mach contours coming off from the interface of the jet shear layer and the terminal shock. A contributor to the noted unsteadiness for DPLR could be the use of point-matched grids, which can limit grid resolution and grid alignment near large gradients. The locations of the terminal shock, interface and bow shock (Table 2) agree well between the three codes, and are consistently 22% larger than the test data.

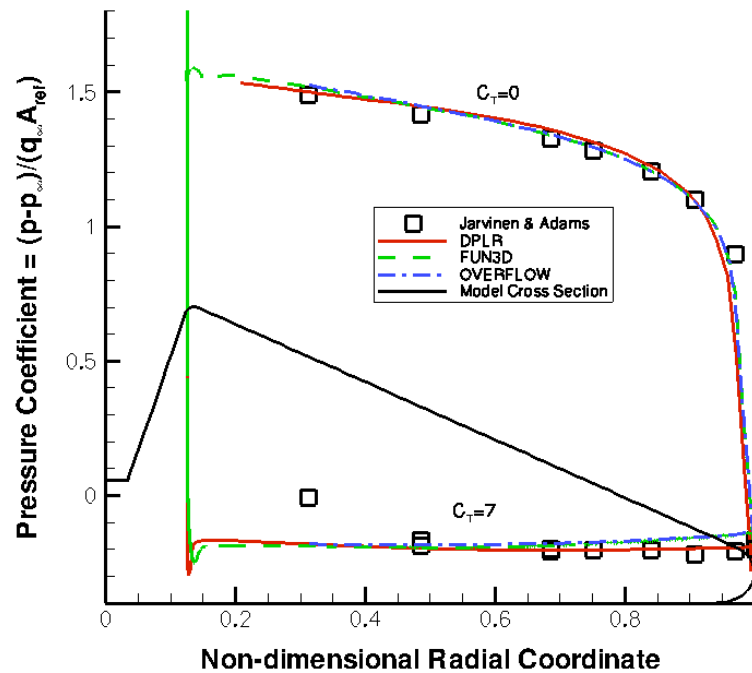


Figure 4: Pressure coefficient of $C_T=0$ and $C_T=7$ for DPLR (red solid line), FUN3D (green dashed line) and OVERFLOW (blue dash-dot line) as compared with Jarvinen and Adams (black square) single-nozzle test data. The black line represents the model cross-section, with the single jet firing upwards in this orientation.

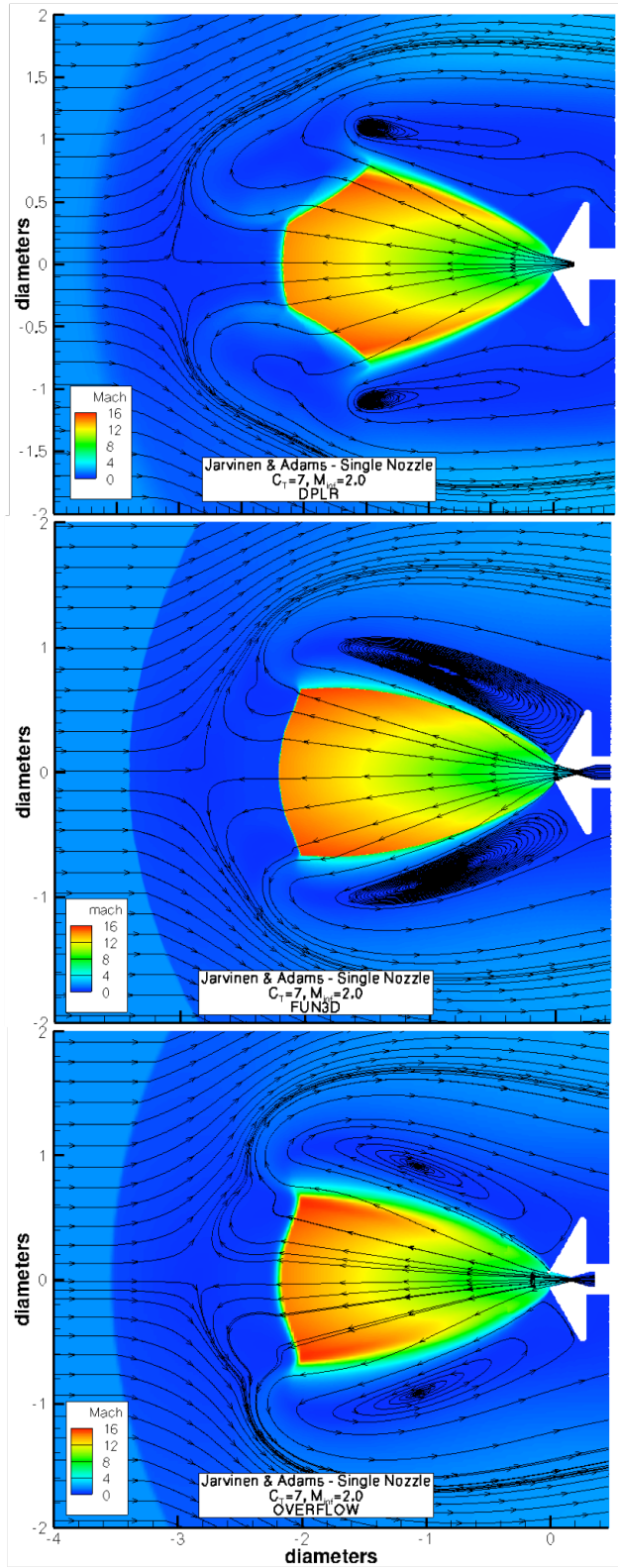


Figure 5: Mach contours of Jarvinen and Adams single-nozzle $C_T=7$ for DPLR (top), FUN3D (middle) and OVERFLOW (bottom).

Table 2: Characteristic distances in model diameters of flow features for all CFD codes and Jarvinen and Adams for the single-nozzle configuration, $C_T=7$.

Source	Bow Shock	Stagnation Interface	Jet Terminal Shock
Jarvinen and Adams	2.9	2.3	1.8
DPLR	3.5	2.8	2.2
FUN3D	3.4	2.8	2.2
OVERFLOW	3.5	2.9	2.2

Grid resolution was found to be extremely important to properly capture the complex flow physics. For example, under-resolving the barrel shock/shear layer can lead to a Mach-reflection jet termination structure and under-resolving the jet termination shock area can result in a completely different plume shape with no termination shock whatsoever. The grid systems for each of the codes are seen in Figure 6. The differences in the resolution and alignment of each grid system is apparent. Although the DPLR grid is more refined than both FUN3D and OVERFLOW, the solution has more unsteadiness and the termination shock appears more diffuse due to averaging of the solution. The alignment of the DPLR grid was done manually before the solution was obtained. The FUN3D feature-based adaption is apparent. The solution is steady and the plume remains in place with the alignment. The OVERFLOW grid has no alignment to the solution. It produces an unsteady solution as well.

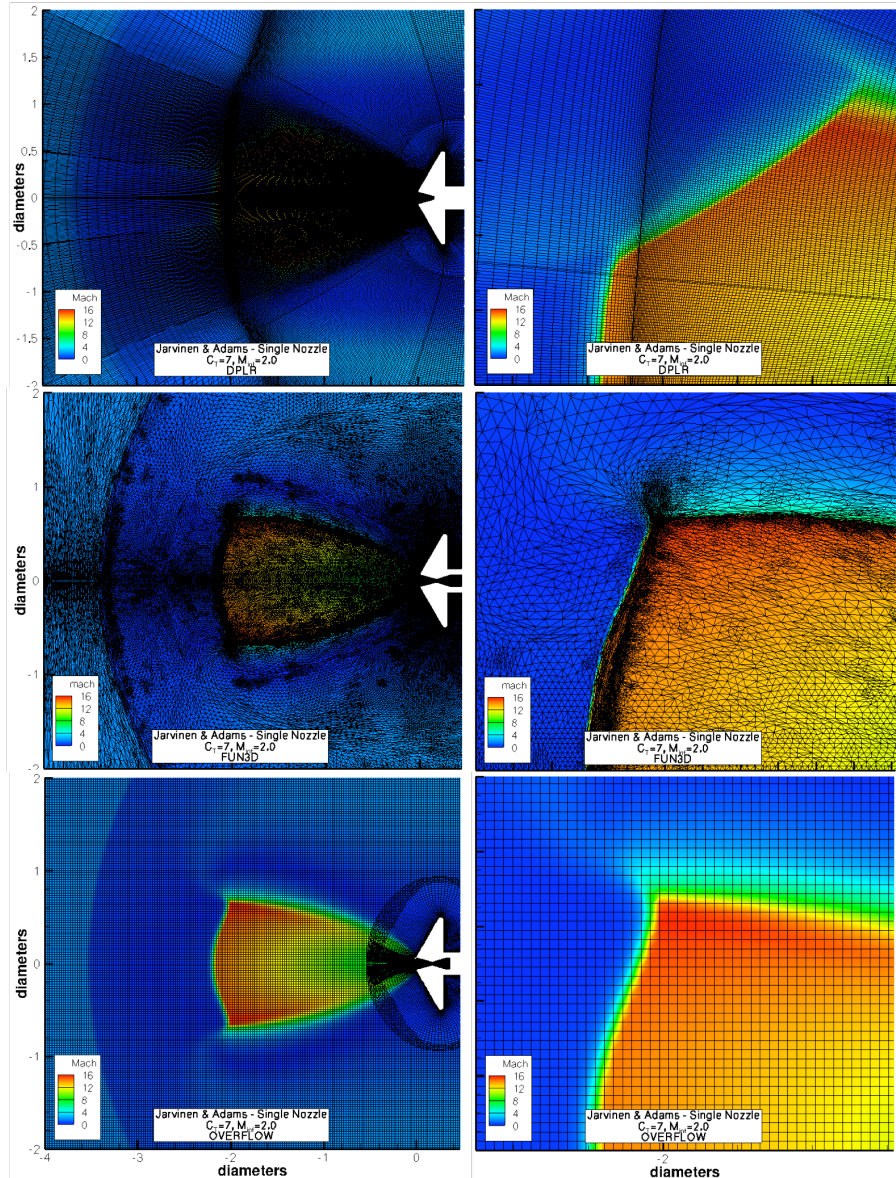


Figure 6: Grid structure for DPLR (top), FUN3D (middle) and OVERFLOW (bottom) on the Jarvinen and Adams single-nozzle $C_T=7$ case. The column on the right is a close-up view of the plume's top corner.

Three-nozzle Configuration

The three-nozzle configuration was analyzed at thrust coefficients 0, 1, 4 and 7. Due to gridding demands, and unstable solutions, only FUN3D and OVERFLOW are presented for the three-nozzle configuration. The pressure coefficient comparisons are made in Figure 7. These comparisons are made along a radial cut that lies at $\phi=90^\circ$. (The nozzles are located at 0° and $\pm 120^\circ$.) The two codes agree with each other in the jet-off case ($C_T=0$). Jarvinen and Adams did not report any pressure coefficient data for the jet-off case. For reference, the vehicle outline is shown as a black line in the $C_T=0$ plot. The comparison at thrust coefficient $C_T=1$ shows good

agreement between the codes and the test data near the nose and along the flank. There is a 21% maximum difference between the test data and the CFD. The codes significantly over-predict the pressure coefficient data for $C_T=4$ on the entire model front face with 104% maximum difference. The agreement with the test data improves at $C_T=7$, except at the nose where there is 200% difference. At the higher C_T the pressure coefficient becomes nearly constant at the outer flank of the model, which was also observed for the single nozzle case. The source of the level of disagreement at $C_T=4$ is currently not known but might be due to differences in the large separation region that encompasses most of the forebody when the jets are firing.

Surface contour plots of the pressure coefficient for all three-nozzle cases by FUN3D and OVERFLOW are shown in Figure 8. As expected there is agreement between FUN3D and OVERFLOW at $C_T=0$. For the $C_T=4$ case, the OVERFLOW solution predicts higher pressure coefficients at the locations between nozzles than the FUN3D solution at $C_T=4$. The nearly constant pressure coefficient on the flank at $C_T=7$ is visible in the contour plots. For all thrust coefficients FUN3D predicts higher pressure coefficients in the vicinity immediately around the nozzles due to lack of grid resolution around the jet exit, which accentuates the node-based solution averaging of interior (high pressure) and exterior (low pressure) values.

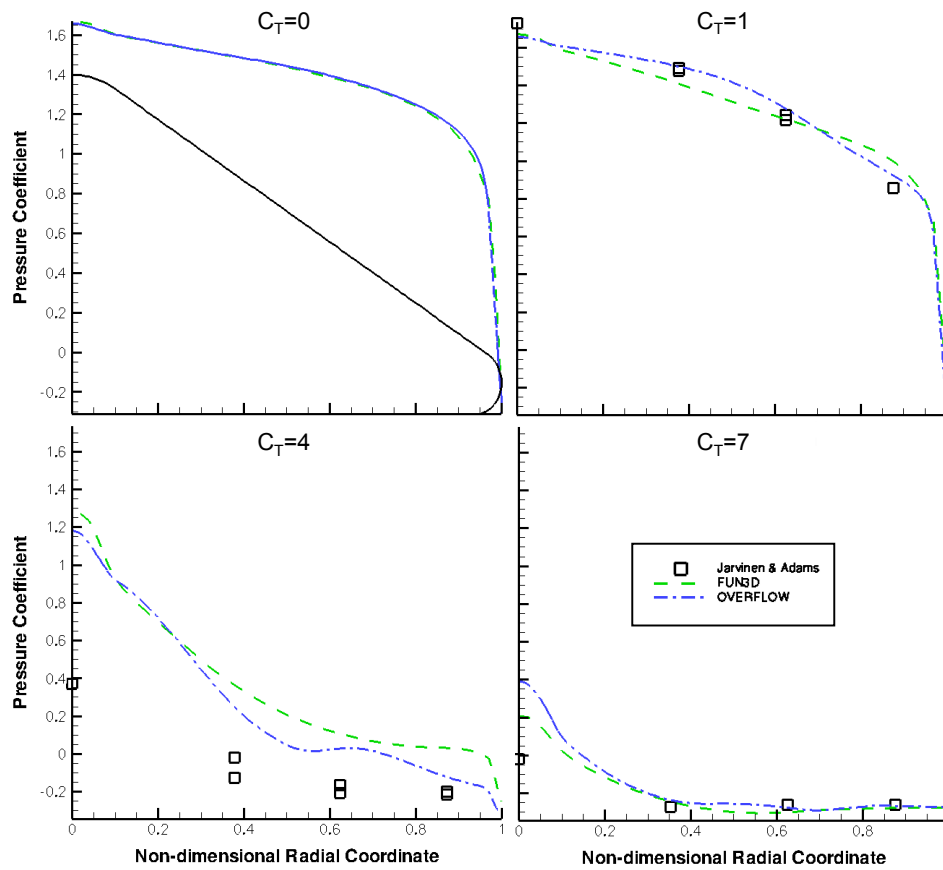


Figure 7: Pressure coefficient of Jarvinen and Adams (black square) three-nozzle configuration for $C_T = 0, 1, 4,$ and 7 compared with FUN3D (green dashed line) and OVERFLOW (blue dash-dot line) along a radial line starting at the nose and ending at the shoulder and oriented 90 degrees clockwise from the top nozzle. The black line represents the model cross-section.

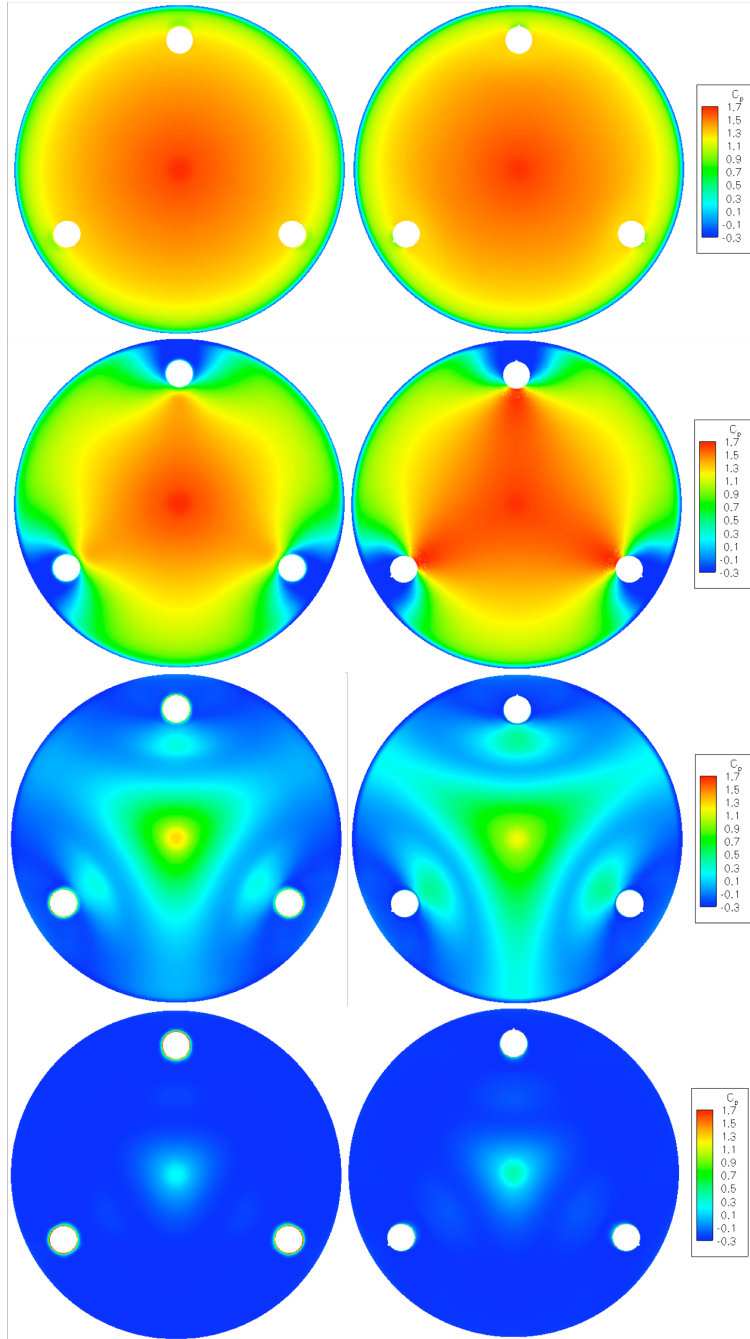


Figure 8: Pressure Coefficient contours predicted by FUN3D (left) and OVERFLOW (right) for the Jarvinen and Adams three-nozzle configuration at thrust coefficients 0, 1, 4 and 7 (top to bottom).

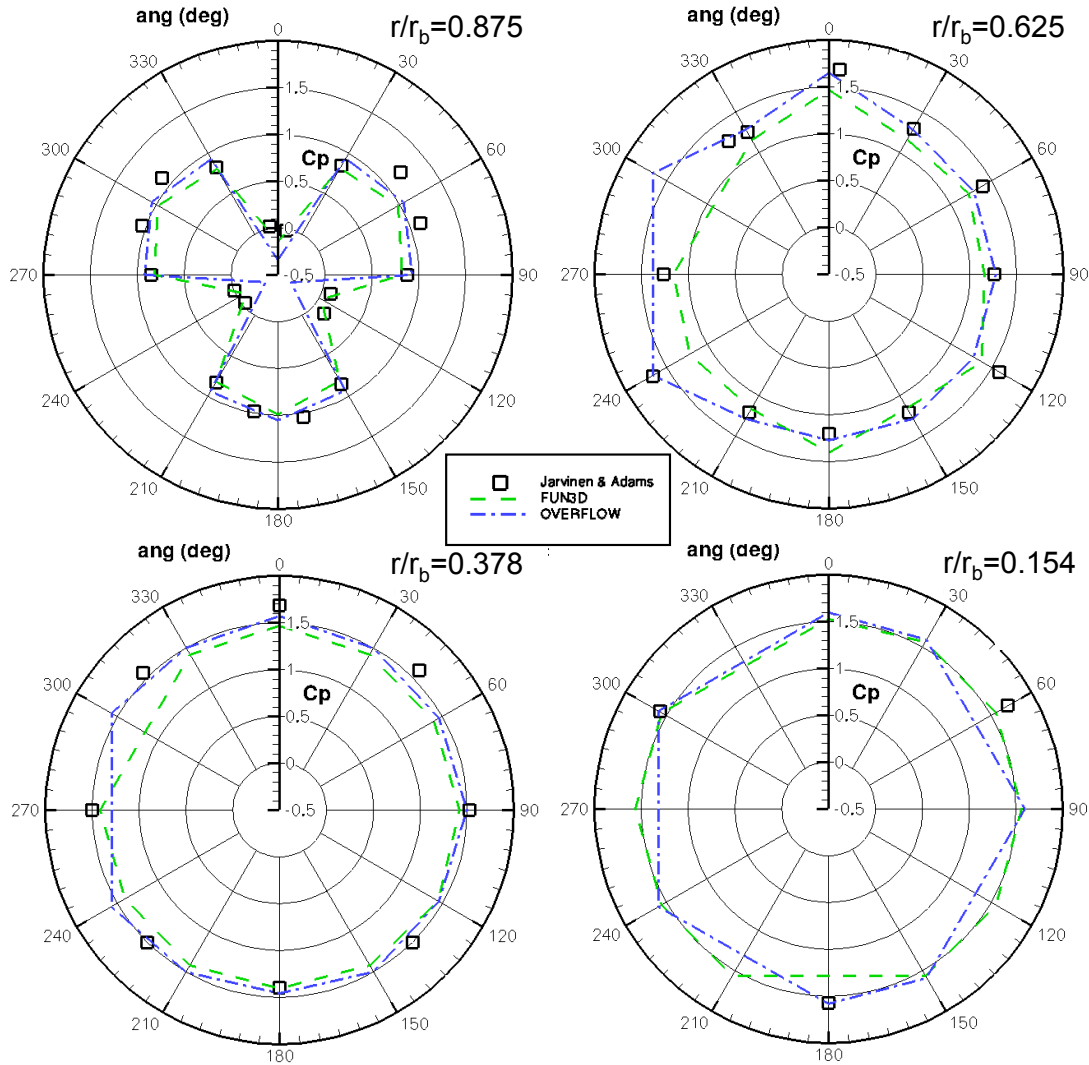


Figure 9: Circumferential pressure distribution at four radial locations for the Jarvinen and Adams three-nozzle configuration at $C_T=1$ at four non-dimensional radial locations ($r/r_b=0.875$, 0.625 , 0.378 , and 0.154). The Jarvinen & Adams test data is shown as black squares, FUN3D as a green dashed line, and OVERFLOW as a blue dash-dot line.

The circumferential pressure distribution for $C_T=1$ is shown in Figure 9 at four non-dimensional radial locations. The radial line nearest to the nozzles, $r/r_b=0.875$, shows the same pressure coefficient trend between test data and CFD. The maximum difference between test data and CFD at this radial location is 31%. The plumes have the most influence on pressure coefficient at this radial location than the others. At the nozzle locations ($\theta = 0, 120$, and 240 degrees) the pressure coefficient drops significantly and in some instances is negative. At $r/r_b=0.625$, 0.378 , and 0.154 the pressure coefficients are nearly constant. The maximum difference between test data and CFD at $r/r_b=0.625$ is 22%, at $r/r_b=0.378$ is 25% and at $r/r_b=0.154$ is 26%.

The Mach contours for the three-nozzle configuration are shown in Figure 10. The jet-off case ($C_T=0$) is simple blunt body flow with cavities at the nozzle locations

and the two codes are in agreement. The Mach contours for a C_T of 1, 4, and 7 are shown on a log scale. At $C_T=1$ OVERFLOW predicts the termination shock further from the body, which in turn pushes the bow shock out further. The subsonic region behind the plume extends out further as a result. The subsonic region directly behind the model has the same shape with both codes, however the FUN3D wake is larger. In the $C_T=4$ case OVERFLOW again predicts a larger plume which also has expanded more at the jet boundaries. The subsonic region behind the plume covers more area in the OVERFLOW solution. As the thrust coefficient is increased a terminal shock begins to form. The two codes agree better with one another for the $C_T=7$ case, yet the stream coming up over the plume is more pronounced in the OVERFLOW. For both $C_T=4$ and 7 the FUN3D bow shock is more normal to the freestream flow. The OVERFLOW solution shows indentation in the bow shock at the plume region. Both codes demonstrate the similar flow characteristics but the OVERFLOW solutions give larger plume interactions.

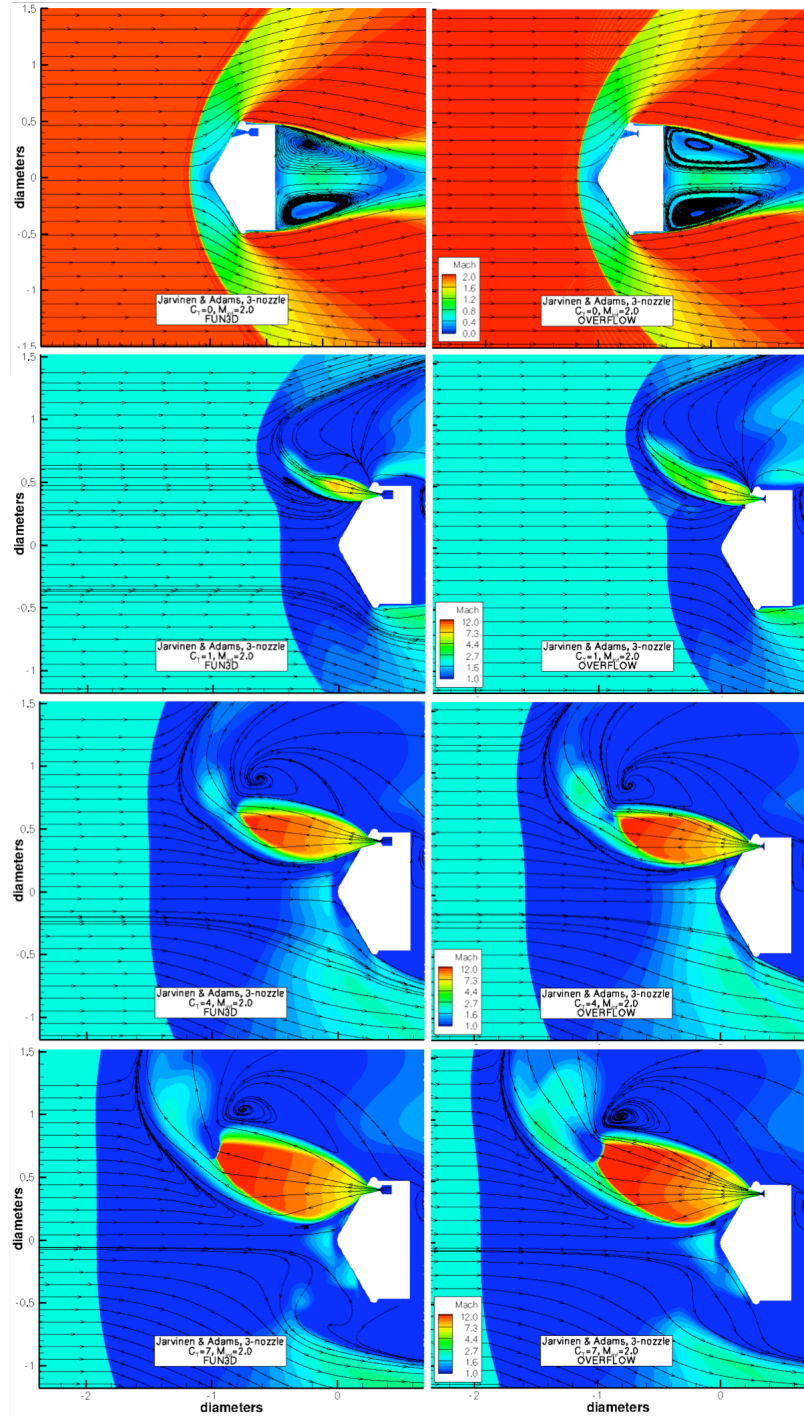


Figure 10: Mach contours from FUN3D (left) and OVERFLOW (right) for $C_T = 0, 1, 4,$ and 7 (top to bottom) of the Jarvinen and Adams three-nozzle configuration.

B. Daso

The SRP experiments of Daso et al⁴ were performed on a 2.6%-scale Apollo capsule (4" diameter) with a single-nozzle configuration. The purpose of these experiments was to examine whether counterflowing jets could be used to reduce aerothermal loads and wave drag rather than enhance drag for entry deceleration,

as is the case for SRP applications. The freestream Mach numbers of the NASA Marshall trisonic blowdown wind tunnel test conditions were Mach 3.48 and Mach 4.0. The exhaust gas of the nozzle was air. Pretest CFD analysis of the flowfields was performed and was consistent with the Schlieren images. The test case chosen for simulation was a jet 0.5-inch diameter sonic nozzle at a mass flow rate of 0.5 lb_m/s ($C_T = 0.4$), Mach 3.48 freestream, and zero angle-of-attack.

The pressure coefficients produced by the three codes are shown in Figure 11. Other than Schlieren images, no other test data was available for comparison. Pressure measurements were made but were not released in either the paper or test report. The codes show the same trends in pressure coefficient but differ from each other by up to 15%. The Mach contours are shown against the Schlieren images in Figure 12. All three codes capture the termination and bow shock locations in agreement with the Schlieren images. The bow and termination shocks appear diffuse in the DPLR solution due to averaging. The extent of afterbody separation is very different between the codes. The level of dissipation and grid resolution would influence the separation on the afterbody. Again, the DPLR simulation showed unsteadiness in the plume, however the level of unsteadiness is less for the lower C_T than for the Jarvinen and Adams case. This may explain some of the discrepancy in the bow shock location. No mention is made of observed unsteadiness in the test.

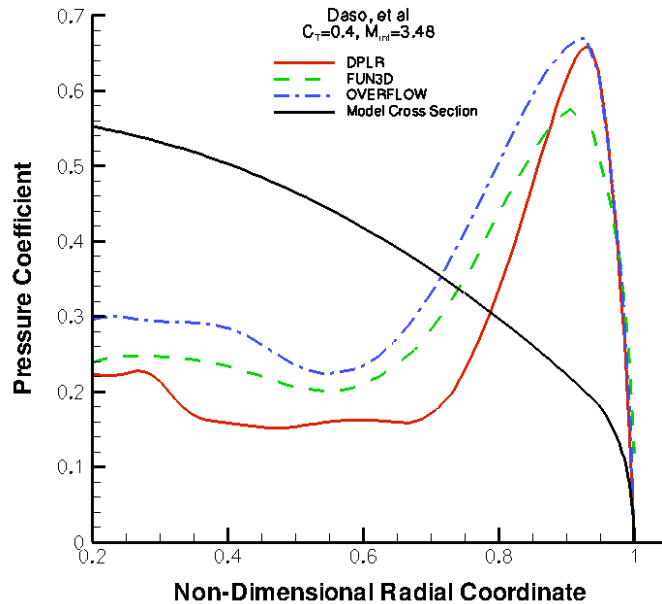


Figure 11: Pressure coefficient of scaled-Apollo capsule experiment by Daso et al at $M_\infty = 3.48$ and $C_T = 0.4$ using DPLR (red solid line), FUN3D (green dashed line) and OVERFLOW (blue dash-dot line) CFD codes. The black line represents the model cross-section.

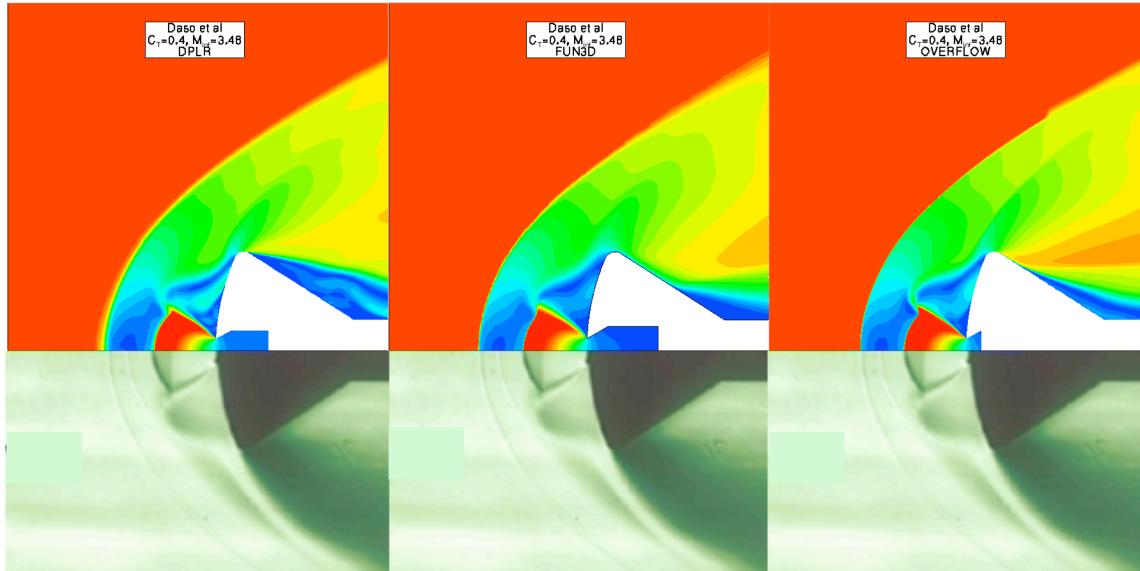


Figure 12: Mach contours from DPLR, FUN3D and OVERFLOW (left to right) compared with Schlieren images from Daso et al for $C_T=0.4$ and $M_\infty=3.48$.

IV. Wind Tunnel Model Design

In order to avoid the issues with using an experiment not specifically designed for CFD validation, future wind tunnel tests are being designed to better capture the quantities and uncertainties necessary for CFD validation.

A next step in validating the CFD methods is to design a wind tunnel test specific to the CFD needs.³⁴ One such test is planned in the Langley Unitary Wind Tunnel (4' by 4' test section) in June 2010. This test will be conducted on a 5-inch diameter 70-degree sphere-cone forebody with the flexibility to test up to four jets at a time. Test data will consist of surface pressure (including high-frequency response), flowfield imagery, and internal pressure and temperature measurements to be used for CFD boundary conditions. The plan is to test at 2.4, 3.5, and 4.6 freestream Mach numbers, a range of thrust coefficients up to 10, and angles of attack up to 20 degrees. The objectives of this wind tunnel test are to provide CFD validation data and to better understand the flow physics including the level of unsteadiness with Schlieren imagery and high-frequency measurements.

Important considerations in the design of the test include tunnel interference and blockage. The model diameter and allowable thrust coefficient both influence whether or not the tunnel walls would affect the pressures seen by the model; and for more extreme cases, whether the tunnel would be blocked causing it to unstart or contaminate the freestream. CFD analyses were performed for model diameters of 4- and 6-inches to estimate model size effects on tunnel interference. FUN3D has demonstrated an ability to quickly turn around solutions of varying parameters, such as modeling tunnel walls, 4- and 6-inch diameter models, thrust coefficients of 0, 5, and 10, and angle-of-attacks of 0, 5 and 10 degrees. In Figure 13 FUN3D has demonstrated the effect of tunnel walls, modeled inviscidly, on surface pressure distributions. The plots are differences in surface pressure between a simulation with and without tunnel walls for $C_T=10$, Mach 4.6, 3.5, and 2.4 and angle of attack 0,

5, and 10. DPLR and OVERFLOW were used on a subset of these cases including an overlapping case for all codes (Figure 14). The results here are similar to the Jarvinen and Adams three-nozzle configuration. FUN3D and OVERFLOW are in agreement and have relatively steady plumes while the plume predicted by DPLR remains unsteady. FUN3D was run with local time stepping, while DPLR and OVERFLOW solutions were advanced with a global time step. The shocks in the DPLR solution appear diffuse due to averaging. From the large database of CFD cases, the model diameter was chosen to be 5 inches after comparing surface pressure differences with and without modeling the tunnel walls and balancing the need for internal packaging volume. The 6-inch diameter case with high C_T appears to create tunnel blockage (Figure 15) that could potentially damage the model instrumentation and reduce productivity. A 5-inch diameter was chosen to alleviate some restriction on allowable C_T and still leave room for internal packaging volume inside the model for instrumentation.

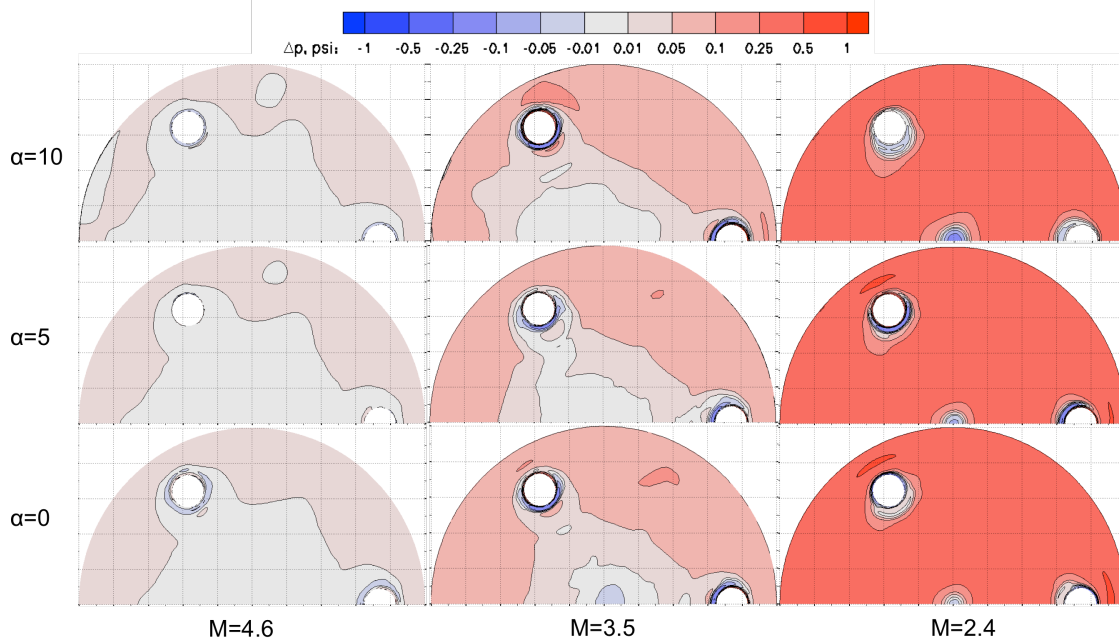


Figure 13: Subset of FUN3D solutions for pre-test wind tunnel model design at Mach 4.6, 3.5, and 2.4 and at angle of attack 10, 5, and 0 for thrust coefficient 10. Contours are surface pressure differences between modeling tunnel walls and not modeling tunnel walls.

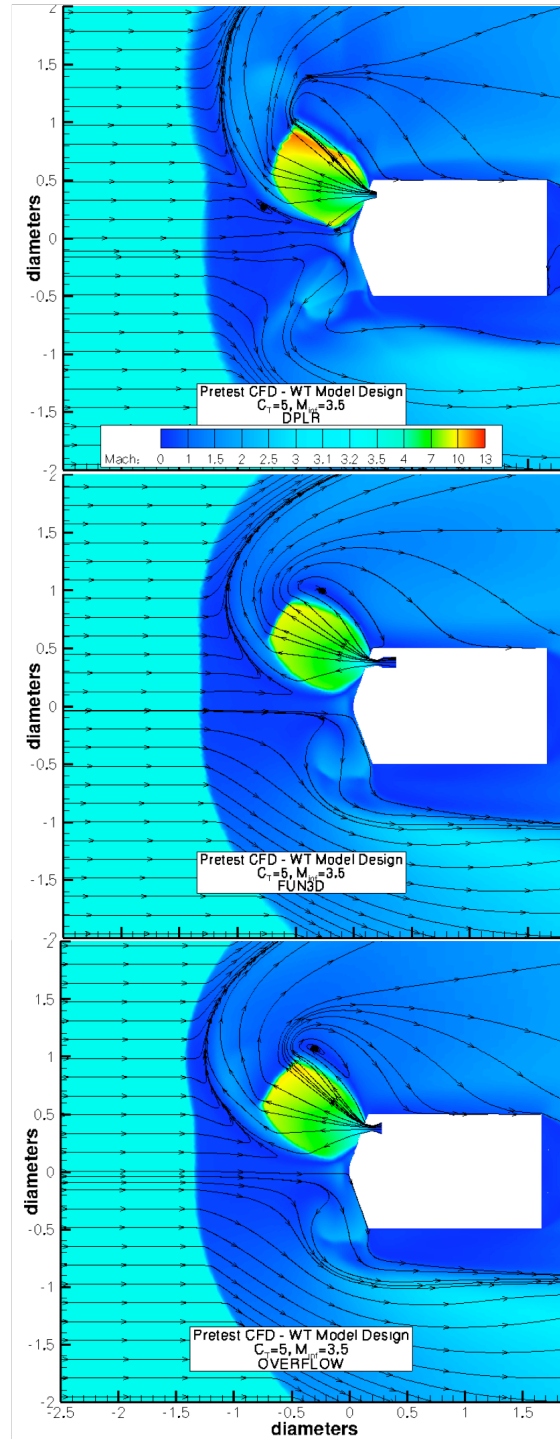


Figure 14: Mach contours for 6-inch diameter wind tunnel model design pre-test case at $M_\infty=3.5$ and $C_T=5$ for DPLR (top), FUN3D (middle) and OVERFLOW (bottom).

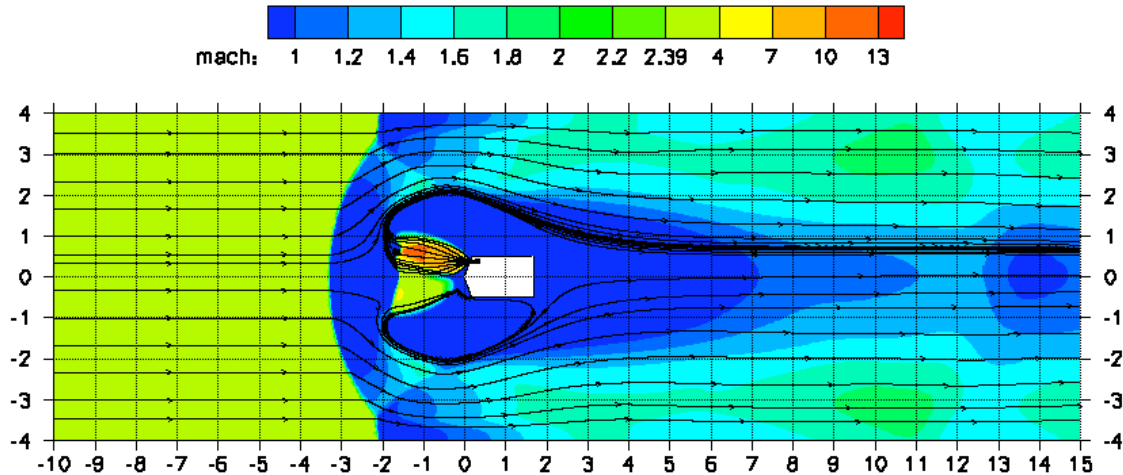


Figure 15: Potential tunnel blockage due to a 6-inch diameter model at $M=2.4$ and $C_T=10$ as predicted with FUN3D.

V. Summary, Conclusions, and Recommendations

The CFD codes DPLR, FUN3D, and OVERFLOW have been exercised for an initial set of SRP test cases from available historical wind tunnel data sets. The CFD test cases include single-jet and three-jet configurations on blunt body wind tunnel models, all at zero degrees angle-of-attack. Comparisons of flow structure and surface pressure between experiment and CFD simulations have been presented. A limited set of conclusions regarding CFD capabilities for SRP can be made based on the test cases run to date. Further assessments and validation exercises will be made with other legacy experiments and once more detailed sets of wind tunnel data become available that address current dataset limitations, especially in the area of data uncertainties and flowfield unsteadiness.

For the two single-jet test cases completed so far, all codes predict similar flowfield structures (jet termination and bow shocks) and match test imagery fairly well where available. However the codes do differ on the level of unsteadiness predicted. The agreement between CFD and measurements of surface pressure vary with freestream Mach number and thrust coefficient. Surface pressure coefficients as predicted by CFD match well with the Jarvinen and Adams test case for a thrust coefficient of 7. Gross flowfield features from the Daso case ($C_T=0.4$) are captured by all codes, but some discrepancies exist in the bow shock location. Unknown effects of unsteady jet interactions may explain some of the discrepancy.

A total of 4 three-jet test cases from the Jarvinen and Adams report were run with FUN3D and OVERFLOW. At low and high thrust coefficients ($C_T=1$ and 7), both codes capture the basic surface pressure coefficient distribution on the model face, except perhaps near the nose. At an intermediate thrust coefficient ($C_T=4$), both codes significantly over-predict the measured surface pressure for unknown reasons but are similar to each other. No supporting imagery was provided to aid further conclusions. The agreement of DPLR with data has not been demonstrated due to grid generation setbacks and unstable solutions.

The FUN3D and OVERFLOW codes seem to agree well between each other for the current set of cases. Although all three codes used the SST turbulence model,

each had a slightly different version of the model. The DPLR SST model is vorticity based while FUN3D and OVERFLOW SST models are strain based. Further work should investigate other turbulence models or improvements needed specifically for SRP. It is difficult to provide more concrete assessments of CFD accuracy because of inconsistencies and omissions in the historical wind tunnel data.

Future studies for SRP CFD need to include a thorough grid sensitivity study or otherwise control grid discretization errors via adjoint-based grid adaptation. With shocks and shear layers being present in the plume structure, care needs to be taken to assure the proper physics are being represented with an adequate level of grid refinement. At some point in the study of SRP, it will be desired to simulate large mass vehicles with liquid-propellant rockets entering the Martian atmosphere. A study needs to be done to understand the sensitivity of chemistry in these types of flows, and if a dependency is established, more capability should be added to properly simulate those cases. Additional code-specific issues and lessons learned are discussed below.

A. DPLR

The DPLR simulations predicted unsteady pulsing plumes, which led to disagreement in plume and shock structures and pressure coefficients with the other codes. All analysis cases performed with DPLR and described here were done with point matched block-zonal grids. The shape of the plume from the retro-propulsion jets is heavily dependent upon the grid alignment and resolution. Future DPLR simulations will explore the use of overset grids, which will allow denser grids in the region of the plume without adding grid points to the overall volume grid. Grid and time resolution studies will also be performed in the future.

B. FUN3D

The FUN3D code can quickly generate this class of flows due to rapid grid generation, which is very beneficial when sampling a wide range of geometry parameters and configurations. Two prominent issues for further advancement include adjoint-based grid adaptation and multi-specie capability. The inability to run adjoint-based grid adaptation is due to FUN3D's lack of an adjoint for the SST turbulence model. (There is an adjoint available for the Spalart-Almaras model, but it does not model free shear layers very well.) If adjoint-based grid adaptation was possible, grid resolution questions could be removed from the list of uncertainties.

C. OVERFLOW

The HLLC++ scheme has been employed, which was written to enhance shock capturing on grids not aligned with the shock. This could be coupled with the Cartesian block adaption scheme in OVERFLOW to capture the plume and bow shock interactions in a more accurate and efficient manner.

In employing the SST turbulence model, it was observed that when using the compressibility correction, presumably unphysical amounts of unsteadiness existed in the flow field. The plume structure pulsated rapidly and showed no signs of damping with more time steps. When not using the compressibility correction, the

plume structure was predominately steady. An increase in unsteadiness was also seen when applying the compressibility correction to the Orion Launch Abort Vehicle with plumes.³⁵ Through these observations, a best practice of not using the compressibility correction was established.

Acknowledgements

Contract numbers NNA04BC25C from NASA Ames Research Center to ELORET CORP. and ESCG/NNJ05HI05C from NASA Johnson Space Center to Jacobs Technology supported part of the work for the present paper. The authors would like to thank the contributions by Ashley Korzun and Chris Cordell with technical advice or comments on the present manuscript. Bil Kleb and Jan-Renee Carlson would also like to thank William Jones of NASA Langley Research Center for extensive geometry and grid generation help and the rest of the FUN3D team for advice and modifications necessary to perform these challenging SRP flow simulations.

References

- ¹ Zang, T. A., "Entry, Descent and Landing Systems Analysis Study: Phase 1 Report," EDL Systems Analysis Team, NASA TM-2010-000002009, May 2010.
- ² Korzun, A.M., Braun, R.D., and Cruz, J.R., "Survey of Supersonic Retropropulsion Technology for Mars Entry, Descent, and Landing," *Journal of Spacecraft and Rockets*, Vol. 46, No. 5, September-October 2009.
- ³ Jarvinen, P.O. and Adams, R.H., "The Aerodynamic Characteristics of Large Angled Cones with Retrorockets," NASA Contract No. NAS7-576, Cambridge, MA, Feb. 1970.
- ⁴ Daso, E. et al, "Dynamics of Shock Dispersion and Interactions in Supersonic Freestreams with Counterflowing Jets," *AIAA Journal* Vol. 47, No. 6, June 2009.
- ⁵ McGhee, R., "Effects of a Retronozzle Located at the Apex of a 140o Blunt Cone at Mach Numbers of 3, 4.5, and 6," NASA TN D-6002, Jan., 1971.
- ⁶ Korzun, A. M., Cordell, Jr., C. E., and Braun, R. D., "Comparison of Inviscid and Viscous Aerodynamic Predictions of Supersonic Retropropulsion Flowfields," *AIAA Paper 2010-5048, 10th AIAA/ASME Joint Thermophysics and Heat Transfer Conference*, Chicago, IL, 30 June-1 July, 2010.
- ⁷ Wright, M.W., White, T., and Mangini, N., "Data Parallel Line Relaxation (DPLR) Code User Manual Acadia - Version 4.01.1," NASA/TM-2009-215388, October 2009.
- ⁸ Buning, P. G., Jespersen, D. C., Pulliam, T. H., Klopfer, G. H., Chan, W. M., Slotnick, J. P., Krist, S. E., and Renze, K. J., "Overflow User's Manual," NASA Langley Research Center, Hampton, VA, 2002.
- ⁹ Anderson, W.K. and Bonhaus, D.L., "An Implicit Upwind Algorithm for Computing Turbulent Flows on Unstructured Grids," *Journal of Computational Physics*, Vol. 128, No. 2, 1996, pp. 391-408.
- ¹⁰ Anderson, W. K., Rausch, R. D., and Bonhaus, D. L., "Implicit/Multigrid Algorithm for Incompressible Turbulent Flows on Unstructured Grids," *Journal of Computational Physics*, Vol. 128, No. 2, 1996, pp. 391-408.
- ¹¹ MacCormack, R.W. and Candler, G.V., "The Solution of the Navier-Stokes Equations Using Gauss-Seidel Line Relaxation," *Computers and Fluids*, Vol. 17, No. 1, 1989, pp. 135-150.
- ¹² Yee, H.C., "A Class of High-Resolution Explicit and Implicit Shock Capturing Methods," NASA TM 101088, Feb. 1989.
- ¹³ Edwards, J. R., "A Low-Diffusion Flux-Splitting Scheme for Navier-Stokes Calculations," *Computers & Fluids*, Vol. 26, 1997, pp. 653-659.
- ¹⁴ Van Albada, G. D., B. Van Leer, B., and Roberts, W. W., (1982), "A Comparative Study of Computational Methods in Cosmic Gas Dynamics," *Astron. Astrophysics*, Vol. 108, 1982, p. 76.
- ¹⁵ Menter, F. R., "Two-Equation Eddy-Viscosity Turbulence Models for Engineering Applications," *AIAA Journal*, Vol. 32, No. 8, 1994, pp. 1598- 1605.
- ¹⁶ Park, M. A., "Anisotropic Output-Based Adaptation with Tetrahedral Cut Cells for Compressible Flows," Ph.D. thesis, Massachusetts Institute of Technology, Sept. 2008.
- ¹⁷ Park, M. A. and Darmofal, D., "Parallel Anisotropic Tetrahedral Adaptation," *AIAA Paper 2008-917*, 2008.
- ¹⁸ Benek, J. A., Buning, P. G., and Steger, J. L., "A 3-D Chimera Grid Embedding Technique," *AIAA Paper 85-1523*, 1985.
- ¹⁹ Chan, W.M., Gomez III, R.J., Rogers, S.E., and Buning, P.G., "Best Practices in Overset Grid Generation," *AIAA-2002-3191*, June 2002.
- ²⁰ Jespersen, D.C., Pulliam, T.H., and Buning, P.G., "Recent Enhancements to OVERFLOW (Navier-Stokes Code)," *AIAA-97-0644*, Jan. 1997.
- ²¹ Tramel, R., Nichols, R., and Buning, P.G., "Addition of Improved Shock-Capturing Schemes to OVERFLOW 2.1," *AIAA-2009-3988*, 19th AIAA Computational Fluid Dynamics, San Antonio, Texas, June 22-25, 2009.
- ²² Pulliam, T.H., and Chaussee, D.S., "A Diagonalized Form of an Implicit Approximate Factorization Algorithm," *J. Comp. Physics*, Vol. 39, 1981.
- ²³ Nichols, R., Tramel, R., and Buning, P., "Solver and Turbulence Model Upgrades to OVERFLOW 2 for Unsteady and High-Speed Applications," *AIAA-2006-2824*, June 2006.

-
- ²⁴ Pandya, S.A., Venkateswaran, S., and Pulliam, T.H., "Implementation of Preconditioned Dual-Time Procedures in OVERFLOW", AIAA-2003-0072, Jan. 2003.
- ²⁵ Baldwin, B.S., and Barth, T.J., "A One-Equation Turbulence Transport Model for High Reynolds Number Wall-Bounded Flows," AIAA-91-0610, Jan. 1991.
- ²⁶ Spalart, P.R., and Allmaras, S.R., "A One-Equation Turbulence Model for Aerodynamic Flows," AIAA-92-0439, Jan. 1992.
- ²⁷ Menter, F. R., "Two-Equation Eddy-Viscosity Turbulence Models for Engineering Applications," AIAA Journal, Vol. 32, No. 8, 1994, pp. 1598– 1605.
- ²⁸ Meakin, R.L., "Object X-Rays for Cutting Holes in Composite Overset Structured Grids," AIAA-2001-2537, June 2001.
- ²⁹ Jespersen, D.C., "Parallelism and OVERFLOW," NAS Technical Report NAS-98-013, NASA Ames Research Center, Moffett Field, CA, Oct. 1998.
- ³⁰ Meakin, R.L., "Automatic Off-Body Grid Generation for Domains of Arbitrary Size," AIAA-2001-2536, June 2001.
- ³¹ Meakin, R.L., "An Efficient Means of Adaptive Refinement within Systems of Overset Grids," AIAA-95-1722, June 1995.
- ³² Murman, S., Chan, W.M., Aftosmis, M.J., and Meakin, R.L., "An Interface for Specifying Rigid-Body Motions for CFD Applications", AIAA-2003-1237, Jan. 2003.
- ³³ Meakin, R.L., "Multiple-Body Proximate-Flight Simulation Methods," AIAA-2005-4621, June 2005.
- ³⁴ Aeschliman, D. P. and Oberkampf, W. L., "Experimental Methodology for Computational Fluid Dynamics Code Validation", AIAA Journal, Vol. 36, No. 5, pp 733-741, May 1998.
- ³⁵ Childs, R., Garcia, J., Stremel, P., Shestopolov, A., "OVERFLOW Simulations of LAV Flow Fields Validation Studies on 60-AA Experiment and Extrapolation to Flight Abort Motor Plumes," Project Orion Internal Report, AR-99, EG-CAP-10-6, January, 2010.